Results in Chemistry 5 (2023) 100716

Contents lists available at ScienceDirect

Results in Chemistry

journal homepage: www.sciencedirect.com/journal/results-in-chemistry

Sulfamethoxazole: Molecular docking and crystal structure prediction

David Stephen Arputharaj [a,*], Meenashi Rajasekaran [b], P.V. Nidhin [c]

[a] Department of Physics, PSG College of Arts and Science, Coimbatore, Tamil Nadu, India
[b] Department of Physics, Kandaswami Kandar's College, Velur 638182, Tamil Nadu, India
[c] Department of Physics, Safa College of Arts and Science, Valanchery 676552, Kerala, India

ARTICLE INFO

Keywords:
Sulfamethoxazole
Molecular docking
Crystal structure prediction

ABSTRACT

The conformational stability of sulfonamide derivatives was examined in the active site of the Dihydropteroate synthase enzyme. The best-docked conformer was identified via the molecular docking approach. Possible stable packing of best-docked conformer was predicted and evaluated from the intermolecular interactions. Further, the interactions of stable conformers with the active site residue were characterized by charge density analysis based on Bader's Quantum Theory of Atoms in Molecules.

Introduction

The folP gene encodes the enzyme dihydropteroate synthase (DHPS), which converts p-aminobenzoic acid (pABA) and 6-hydroxymethyl-7,8-dihydropterin-pyrophosphate into 7,8-dihydropteroate (DHPP). Because higher eukaryotes lack the folate pathway, this reaction is an important step in the biosynthesis of folate in bacteria and primitive eukaryotes. This makes it a promising target for the development of antimicrobial drugs [1]. The highly successful sulfa medications that have been in use for more than 70 years are directed against DHPS. However, the development of sulfa drug resistance has severely reduced their usefulness [2,3] and has spurred numerous attempts to create new families of DHPS inhibitors [4]. Sulfonamides are extensively used as antibiotic drugs [5] for treating infections triggered by fungi and protozoa. However, there exist non-antibiotic sulfonamides [6], wherein they have been deployed for treating diabetes. Drugs in the sulfa class inhibit the formation of the folate intermediate 7,8-dihydropteroate by inhibiting the enzyme dihydropteroate synthase (DHPS) [7], which catalyzes the condensation of 6-hydroxymethyl-7,8-dihydropterin-pyrophosphate (DHPP) with p-aminobenzoic acid (pABA) in the production of folate [8]. The sulfa medication sulfamethoxazole (SMX) in conjunction with the DHFR inhibitor trimethoprim is an effective treatment for a wide variety of bacterial infections [9]. Sulfonamide-based medicines were once first-line alternatives, but they have been pushed to the sidelines because of the prevalence of DHPS mutations in many clinical isolates.

The catalytic and resistance mechanisms of DHPS have been the subject of structural, computational, and mutagenesis research, according to Yun et al [10]. They were able to structurally identify important steps in the enzyme-catalyzed process in crystalline DHPS. The production of a novel cationic pterin intermediate by the S(N)1 reaction is supported by the results. They further demonstrate that during catalysis, two conserved loops produce a substructure that develops a distinct binding pocket for p-aminobenzoic acid, one of the two DHPS substrates. The roles of the conserved active-site residues are explained by this substructure, which also explains how sulfonamide resistance develops, along with the pterin-binding pocket.

These drugs were also used widely for treating the infections in the urinary tract caused by the bacteria Escherichia Coli (E.Coli) and they are considered as a frontline treatment for pneumonia observed in AIDS patient [11]. The present study focuses on the conformational stability of 24 variants of sulfonamide drugs [Fig. 1] in the active site of the DHPS enzyme. The stable packing of best-docked drug was predicted through *ab initio* methods and the intermolecular interaction of the inhibitor molecule in the active site of the DHPS enzyme was analyzed. Further, the charge density analysis has been carried out via Bader's Quantum Theory of Atoms in Molecule (QTAIM) [12], to characterize the bonds.

Materials and methods

Molecular docking

The coordinates of all 24 ligands were obtained from the reported crystal structures. The crystal structure of DHPS in the complex form [1AJ0] was obtained from the Protein data bank. The protein Preparation Wizard tool [13] was used for preparing the enzyme and before the

* Corresponding author.
E-mail address: stevepearlin@gmail.com (D.S. Arputharaj).

https://doi.org/10.1016/j.rechem.2022.100716
Received 15 September 2022; Accepted 5 December 2022
Available online 6 December 2022

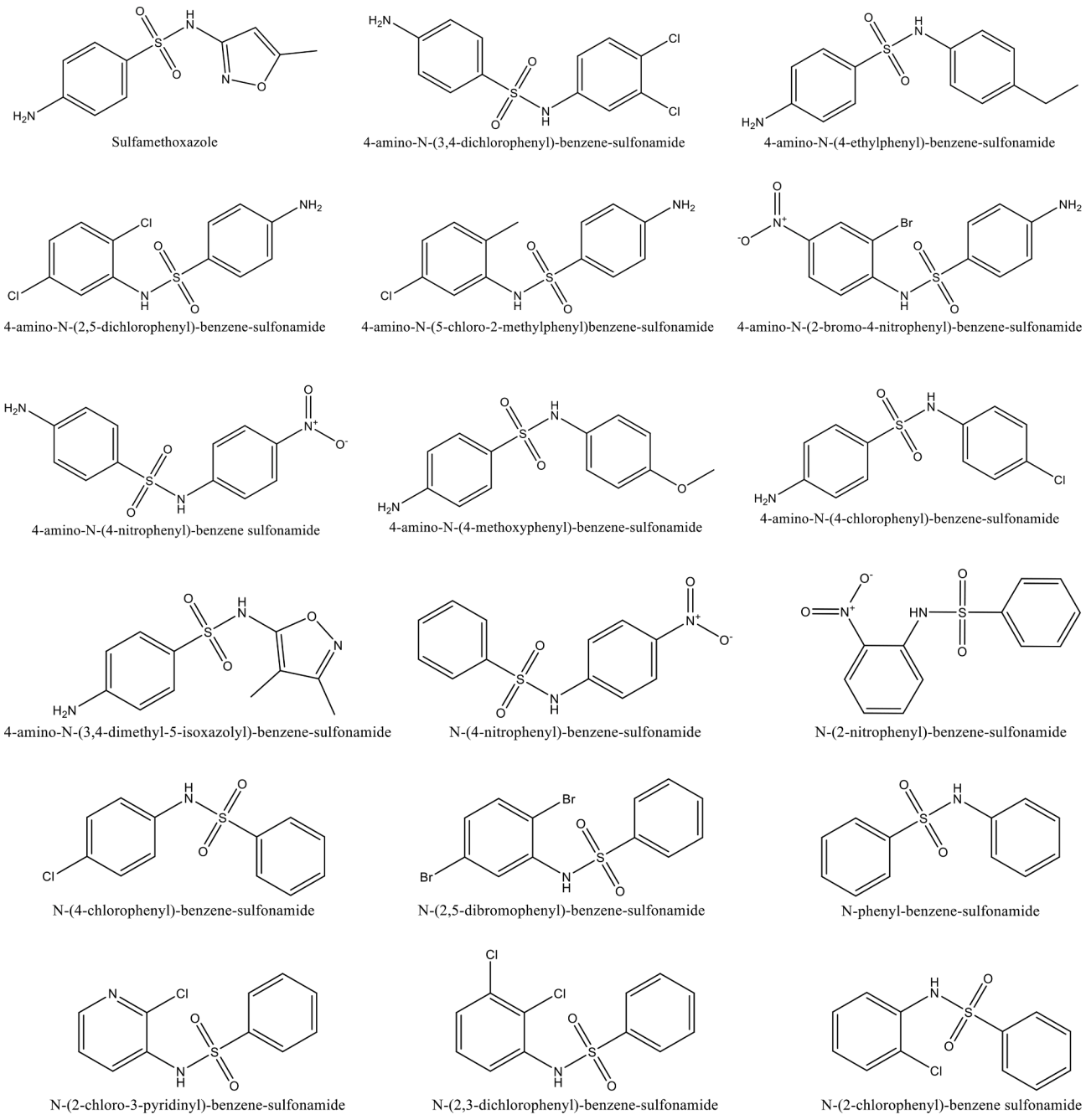

Fig. 1. The chemical structures of sulfonamide drugs.

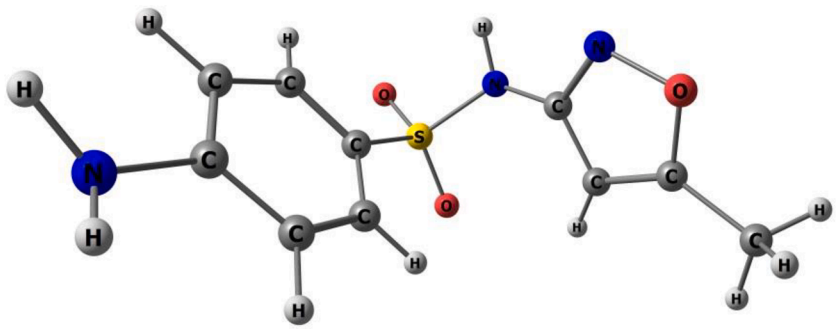

Fig. 2. Sulfamethoxazole.

Table 1
Induce Fit docking score values of SMA-DHPS complex.

Sulfonamide Derivatives	docking score	glide gscore	glide emodel	glide energy (KJ/mol)	Prime Energy (KJ/mol)	IFD Score
Sulfamethoxazole (SMA)	−6.637	−6.637	−72.265	−202.66	−48580.8	−587.19
4-amino-N-(3,4-dichlorophenyl)-benzene-sulfonamide	−5.883	−5.883	−62.86	−196.765	−48510.6	−585.6
4-amino-N-(4-ethylphenyl)-benzene-sulfonamide	−6.609	−6.609	−65.867	−191.602	−48390.5	−584.89
4-amino-N-(2,5-dichlorophenyl)-benzene-sulfonamide	−6.127	−6.127	−59.189	−178.268	−48428.1	−584.86
4-amino-N-(4-nitrophenyl)-benzene sulfonamide	−6.105	−6.105	−59.353	−189.012	−48424.8	−584.8
4-amino-N-(2-bromo-4-nitrophenyl)-benzene-sulfonamide	−5.688	−5.688	−61.634	−195.2	−48452.4	−584.71
4-amino-N-(5-chloro-2-methylphenyl)benzene-sulfonamide	−6.122	−6.122	−53.777	−174.285	−48400.1	−584.52
4-amino-N-(4-methoxyphenyl)-benzene-sulfonamide	−5.682	−5.682	−55.148	−173.105	−48427.7	−584.41
4-amino-N-(4-chlorophenyl)-benzene-sulfonamide	−5.688	−5.688	−61.644	−193.61	−48423.9	−584.37
4-amino-N-(3,4-dimethyl-5-isoxazolyl)-benzene-sulfonamide	−6.436	−6.436	−73.446	−206.748	−48360.3	−584.36
N-(4-nitrophenyl)-benzene-sulfonamide	−5.636	−5.636	−58.85	−185.698	−48294.7	−582.77
N-(2-nitrophenyl)-benzene-sulfonamide	−5.415	−5.415	−50.652	−160.419	−48270	−582.25
N-(4-chlorophenyl)-benzene-sulfonamide	−5.532	−5.532	−48.872	−157.553	−48231.9	−581.92
N-(2,5-dibromophenyl)-benzene-sulfonamide	−5.059	−5.059	−53.576	−179.209	−48211.4	−581.2
N-phenyl-benzene-sulfonamide	−5.613	−5.613	−55.69	−174.808	−48133.6	−580.82
N-(2-chloro-3-pyridinyl)-benzene-sulfonamide	−5.425	−5.425	−53.847	−174.126	−48113.9	−580.4
N-(2,3-dichlorophenyl)-benzene-sulfonamide	−5.282	−5.282	−47.633	−157.754	−48116	−580.28
N-(2-chlorophenyl)-benzene sulfonamide	−5.321	−5.321	−46.664	−153.942	−48108.9	−580.23

docking study, the water molecules and ions were removed from the complex. Ligprep Module [14] was incorporated for preparing all the ligands and the Induced Fit docking approach [15] was employed for the docking process. Among the 24 ligands, the sulfamethoxazole (SMA), [Fig. 2] was found to have the best docking score and this lowest energy complex was considered for further analysis. The docking score values of all the ligands were listed in Table 1. The intermolecular interactions between SMA and DHPS were visualized by Maestro and PyMol [16].

Crystal structure prediction

The geometry of the parent molecule was initially optimized in the gas phase using the DFT [17] method via B3LYP/6–31 g(d) basis set operations with the Gaussian 09 software [18]. Using the MOLPAK package [19], the common space groups *P*1, *P*-1, *P*2, *Pm*, *Pc*, *P*21, *P*2/*c*, *P*21/*m*, *P*2/*m*, *P*21/*c*, *Cc*, *C*2, *C*2/*c*, *Pnn*2, *Pba*2, *Pnc*2, P221, *Pmn*21, *Pma*2, *Pca*21, *Pna*21, *Pnma*, and *Pbca* were searched for dense crystal packings. By executing sequential orientations of the core parent molecule in all frequent coordination geometries and creating the necessary coordination patterns with unit cell volume as a function, the search for dense crystal structures of SMA was conducted globally. From 90° to 90° rotation in 10° steps, the packings of the SMA molecule inside the threshold contacts of the adjacent fragments of the parent molecules were created. In the multidimensional grid, the SMA's direction and repetition led to the creation of 6859 hypothetical structures. The PMIN [19] procedure used the repulsion potential field alone as the inner lattice minimization to minimise the lattice energy of these starting structures. The inner lattice minimizations of the hypothetically densest SMA molecule structures with the smallest cell volume produced in the frequently encountered 31 space groups were carried out using the DMACRYS algorithm [20], which included a repulsion-dispersion potential field of the type (1)

$$U = \sum_{i\in 1k\in 2} \left[\left(A_{ii}A_{kk}\right)^{1/2} \right] \exp\left[-\left(B_{ii} + B_{kk}\right)R_{ik}/2 \right] - \left(C_{ii}C_{kk}\right)^{1/2}/R_{ik}^{6} \qquad (1)$$

where molecules 1 and 2 of different kinds contain atoms i and k, respectively. The FIT potential was parameterized by Williams and Cox [21] with additional terms for the hydrogen atoms bound to nitrogen, which were later fitted by Coombes et al [22], and this potential field was used in the lattice minimization. The inner lattice minimization corrected the disparity of the PMIN lattice minimization with repulsion alone potential, so validating the correctness. The set of multipoles produced by the GDMA [23] method was examined at the MP2 level by MP2/6-31G(d,p) basis set operation. This allowed for a detailed analysis of the electrostatic interactions as well as the intermolecular binding of the SMA molecules. Based on energy ranking, the lattice-minimized SMA molecules that met the Born criterion for mechanical stability and had valid eigenvalue representations were listed in Table 3. The second derivative properties computed from the Cij elements of the Hessian matrix were used to confirm the SMA molecule's thermodynamic stability. In the current study, the nonzero representation from the symmetry requirements was removed to re-minimize the erroneous hypothetical structures produced with negative eigenvalues.

Table 2
Ligand-Protein Interactions.

Interactions	Distance [Å]	Type
ARG63:HE…SMA:O1	2.782	Hydrogen Bond
ARG63:HH21…SMA:O1	1.962	Hydrogen Bond
LYS221:HZ1…SMA:O2	2.047	Hydrogen Bond
ARG255:HH12…SMA:O1	2.283	Hydrogen Bond
ARG255:HH22…SMA:O1	2.680	Hydrogen Bond
SMA:H1…THR62:OG1	1.908	Hydrogen Bond
SMA:H7…ASP185:OD2	1.889	Hydrogen Bond
LYS221:HE3…SMA:O2	3.072	Hydrogen Bond
LYS221:HE3…SMA:N3	3.021	Hydrogen Bond
LYS221:HZ2…SMA:N3	2.252	Hydrogen Bond
LYS221:HZ2…SMA	2.716	Hydrogen Bond;Electrostatic [Pi…Cation; Pi…Donor Hydrogen Bond]
ARG255:NH1…SMA	3.644	Electrostatic [Pi…Cation]
SMA…PHE190	3.617	Hydrophobic [Pi…Pi Stacked]
PHE190…SMA	5.224	Hydrophobic [Pi…Pi T…shaped]
SMC10…PRO64	4.829	Hydrophobic [Alkyl]
PHE190…SMC10	4.029	Hydrophobic [Pi…Alkyl]
SMA…ARG63	4.835	Hydrophobic [Pi…Alkyl]

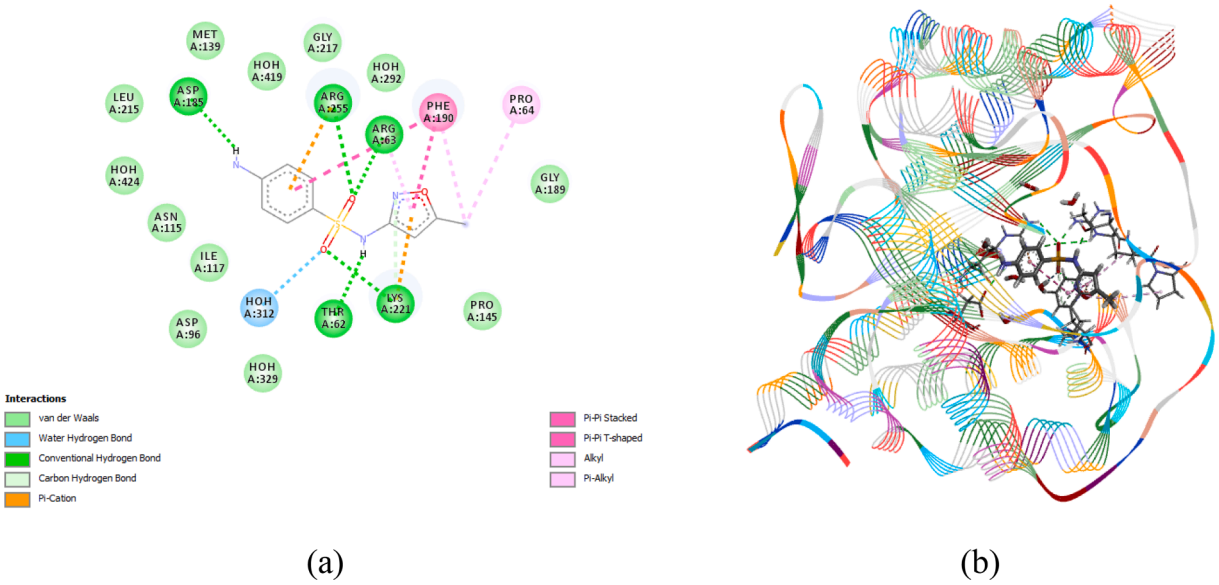

Fig. 3. The SMA-DHPS complex showing (a) 2D and (b) 3D intermolecular interactions.

Table 3
List of Predicted crystal structures together with reproduced experimental structure (Exp).

ID	Space group	$U_{lattice}$ kJ/mol	a (Å)	b (Å)	c (Å)	α()	β()	γ()	Volume	density (g/cm^3)
AK	$P2_1/c$	−152.66	13.59	5.45	15.84	90.00	103.99	90.00	1137.65	1.48
AH	$P21$	−151.41	8.77	5.38	14.07	90.00	68.49	90.00	617.51	1.36
FC	$P21/c$	−150.84	14.71	5.23	16.80	90.00	113.04	90.00	1188.10	1.42
CA	P-1	−148.97	8.16	5.58	13.54	89.53	102.10	75.26	581.52	1.45
FA	$P21/c$	−146.68	8.16	26.85	5.60	90.00	105.55	90.00	1181.96	1.42
AM	$P21/c$	−146.47	8.37	20.27	7.04	90.00	101.78	90.00	1168.04	1.44
BF	Pm	−146.23	14.22	15.45	5.28	90.00	90.00	90.00	1159.96	1.45
AV	$Pna2_1$	−146.18	14.22	15.46	5.28	90.00	90.00	90.00	1160.26	1.45
Exp	***C2/c***	**−145.91**	15.70	5.54	26.93	90.00	90.74	90.00	2343.54	1.44
DD	$C2/c$	−145.91	15.70	5.54	26.93	90.00	90.71	90.00	2343.62	1.44
AB	P-1	−144.14	8.99	6.92	13.35	96.03	128.04	78.29	640.93	1.31
CB	$Pbca$	−143.66	5.53	15.83	27.49	90.00	90.00	90.00	2406.54	1.40
CC	$Pbca$	−143.64	5.53	15.83	27.49	90.00	90.00	90.00	2406.56	1.40
AZ	$P2_12_12_1$	−136.30	12.52	11.09	9.01	90.00	90.00	90.00	1251.26	1.34
CE	$Pbcn$	−135.10	18.50	6.87	18.74	90.00	90.00	90.00	2381.63	1.41
CD	$P2_1$ /c	−135.07	18.51	6.87	18.74	90.00	90.00	90.00	2381.80	1.41
AP	$P2_12_12$	−132.22	13.97	13.60	6.29	90.00	90.00	90.00	1195.31	1.41
AY	$Pca2_1$	−132.12	15.39	8.42	10.01	90.00	90.00	90.00	1297.60	1.30
BH	$Pca2_1$	−132.06	15.43	8.41	10.01	90.00	90.00	90.00	1299.21	1.29
DB	$C2$	−129.49	15.05	7.76	14.00	90.00	58.04	90.00	1386.71	1.21
AQ	$P212121$	−127.21	8.89	13.23	10.13	90.00	90.00	90.00	1190.10	1.41
AS	$Pna2_1$	−124.39	14.15	16.10	5.48	90.00	90.00	90.00	1249.55	1.35
BB	$P1$	−117.17	25.80	8.68	5.66	90.00	90.00	90.00	1267.41	1.33
BA	$P2_12_12$	−116.93	25.78	8.69	5.66	90.00	90.00	90.00	1267.65	1.33
BD	$Pna21$	−113.57	14.71	8.42	10.75	90.00	90.00	90.00	1330.59	1.26
AA	$P1$	−104.01	8.84	5.50	11.94	125.71	56.00	137.22	310.79	1.35
AF	$P2_1$	−100.70	10.39	7.00	9.09	90.00	111.89	90.00	612.95	1.37
DA	Cc	−97.04	10.08	12.79	13.08	90.00	122.32	90.00	1424.46	1.18
AU	$Pna2_1$	−96.08	13.61	5.35	17.94	90.00	90.00	90.00	1304.98	1.29

Results and discussion

SMA-DHPS complex

The DHPS enzyme having 282 residues, is folded into eight α-helix stacked around the outside of nine β-strands. The assessment of the binding affinity of SMA against the active site residues of DHPS was done by molecular docking approach. The binding pocket of DHPS comprises hydrophobic and electrostatic regions framed by ARG63, LYS221, ARG255, THR62, ASP185, PHE190, and PRO64 residues. Moreover, the ligand interaction with protein was predominantly stabilized by 10 hydrogen bonds. The NH, NH_2, and SO_2 groups dominate most of the H-bond interactions with residues. The complete list of interactions in the SMA-DHPS complex was tabulated in Table 2. Fig. 3 poses both the 2D and 3D ligand interaction with protein.

Structure close to real and hydrogen bonding interactions

Table 3 depicts the list of the lattice-minimized crystal structure of SMA molecules encountered for different space groups and they are ranked on basis of energy. From this table, it was clear that the structure, DD, with −145.91 KJ/mol reflects the experimental structure [24] well and the packing is stable at the $C2/c$ spacegroup of monoclinic system, which is highly correlated with the reported X-ray structure [exp]. Fig. 4

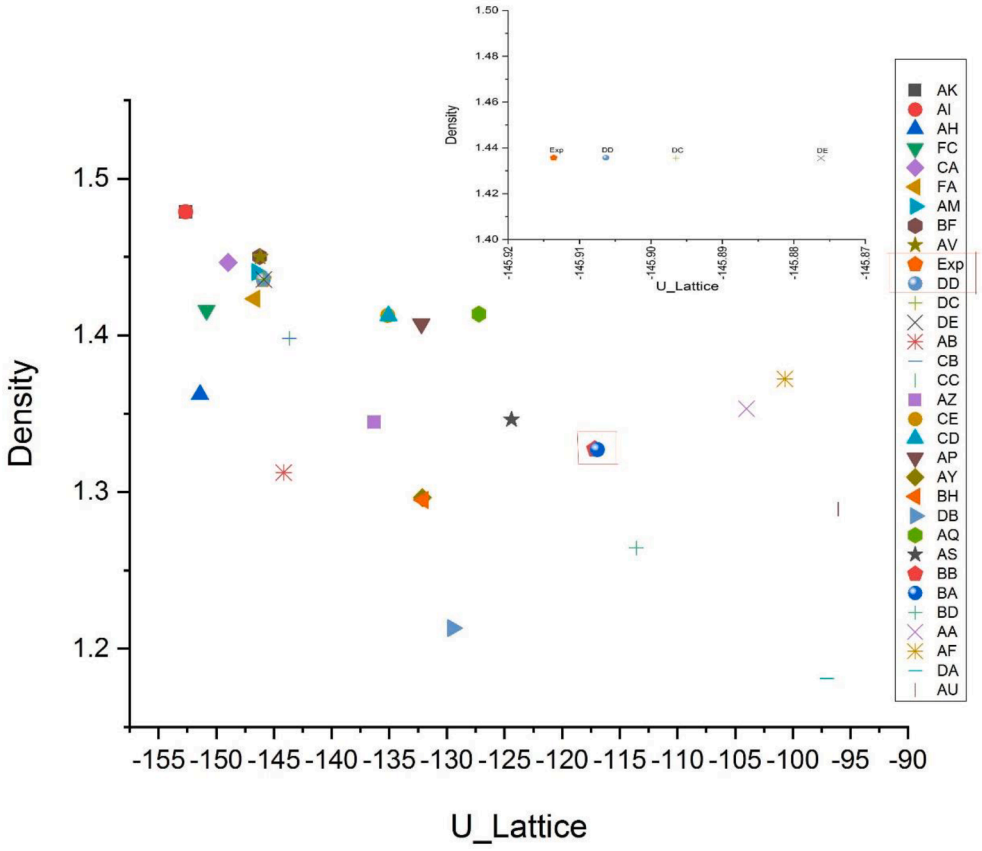

Fig. 4. Energy landscape of predicted crystal structures along with the minimized experimental structure.

Table 4
Intermolecular interactions for predicted (DD) and experimental (EXP) crystal structures.

H-Bond	Donor…Acceptor [Å] DD/EXP	Donor-H……..Acceptor [] DD/EXP
N1-H1…O2	3.5/3.2	164/165
N2-H4…S1	3.3/-	107/-
N2-H4…O2	3.0/-	134/-
N2-H7…O1	2.9/3.3	126/141
N2-H4…O1	3.5/3.3	128/163
C5-H5…O1	3.4/3.6	144/145
C8-H8…N3	3.3/3.2	131/158
C10-H10…O3	3.5/3.7	166/152
C10-H10…N3	3.5/-	142/-
C10-H9…N3	3.6/3.6	142/137

shows the dense crystal energy landscape with the generated optimized crystal structures together with the minimized experimental SMA structure within the region from –97 KJ/mol to –153 kJ/mol. The thermodynamic stability of the predicted structure [DD] was further confirmed by their strong H-bond interactions [Table 4] and the same was compared well with that of the real structure. Moreover, the individual contribution of atoms in the H-bonding interactions was well exploited from the 2D fingerprint plot of Hirshfeld surface (HS) [Fig. 5] using the Crystal Explorer package [25].

The maximum contact contribution towards the total HS surface is identified from O…H/H…O interactions with 30.8 % and 32.8 % for both predicted and experimental crystal structures. These were originated by NH2 groups interacting with oxygen atoms of the SO_2 group [N2-H4…O1, N2-H4···O2, N2-H7···O1], CH of aniline ring and NH group with oxygen atoms of SO2 [C5-H5···O1, N1-H1···O2] and methyl group with the oxygen of isoxazole ring [C10-*H*10···O3]. These were highlighted by sharp spikes at a short distance in the fingerprint plot. Next to this, H···H contacts contribute with 28.9 % (predicted) and 27.8 % (Exp) with the least distance, d(H6, H9) of 2.56 Å for predicted crystal structure, and the equivalent distance in the experimental structure is 2.83 Å. The least contribution is calculated for N···H/H···N interactions involved in the isoxazole ring [C8-H8···N3. C10-H9···N3 and C10-*H*10···N3] and the corresponding percentage values for predicted and experimental crystal structures were 15.8 % and 13.6 % respectively. These interaction contributions were well established from the contact enrichment ratio and %contacts listed in Table 5.

Energy between molecular pairs

The symmetric molecules of the SMA crystal structure of both real and predicted structures were stacked antiparallel and framed the ribbon pattern [Fig. 6]. This orientation was predominantly stabilized by N2-H7···O1 and N2-H4···O2 H-bond interactions. The four main aspects of molecular interaction energy—electrostatic, polarisation, dispersion, and exchange-repulsion were calculated using monomer wavefunctions at B3LYP/6-31G(d,p) levels along with Grimme's D2 dispersion corrections which are incorporated in Crystal Explorer package [25]. The energies of all interactions between the molecular pairs are listed in Table 6 for both predicted and real crystal structures and the values were found to be coherent. Five molecular pairs were identified with significant intermolecular energy, E_{tot} ranges from –23.3 to −38.3 KJ/mol. The first molecular pair is framed from the N2-H4···S1, N2-H4···O2 and N2-H7···O1, H-bond interactions with the total energy of −39.4 KJ/mol [real] and −38.3 KJ/mol [DD]. This molecular pair is highly stabilized from 27 % of electrostatic and 71 % of dispersion energies. 50 % contribution of these energies was found for the second molecular pair stabled from N1-H1···O2 interaction with E_{tot} values were –32.1 KJ/mol and −38.2 KJ/mol for predicted and real crystal structures respectively.

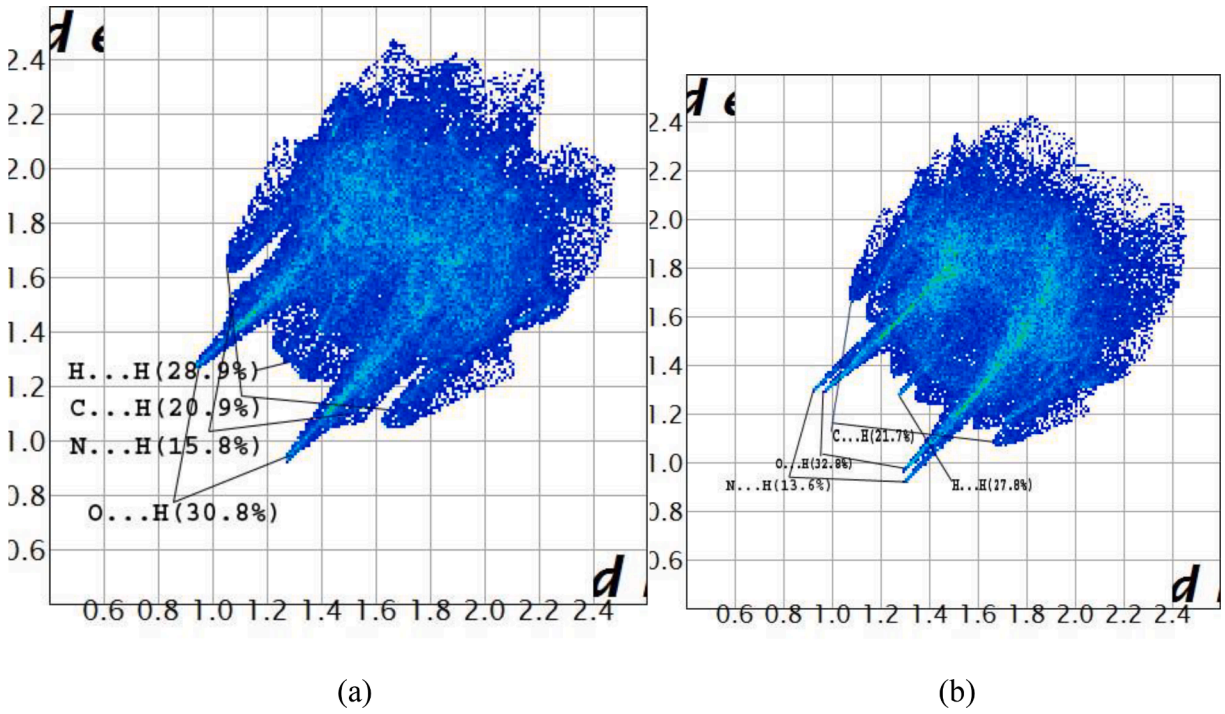

Fig. 5. Fingerprint plot showing the percentage of contact contribution towards the total HS surface for both (a) predicted and (b) Exp crystal structures.

Table 5
Nature of intermolecular contacts on the Hirshfeld surface by chemical types.

DD							EXP						
atom	**H**	**C**	**N**	**O**	**S**	**HC**	**atom**	**H**	**C**	**N**	**O**	**S**	**HC**
Surf%	14.38	23.59	9.89	14.97	2.73	34.45	Surf%	14.6	23.46	9.87	14.78	2.73	34.56
H	1.25						H	1.28					
C	1.26	5.42					C	1.21	5.43			%contacts	
N	0.87	1.26	0.41	%contacts			N	0.84	1.25	0.43			
O	14.38	4.44	0.16	0.21			O	14.36	4.4	0.16	0.22		
S	2.47	0.06	0.63	0	0		S	2.59	0.04	0.57	0	0	
HC	7.23	27.13	14.56	9.51	2.26	6.47	HC	7.19	27.27	14.41	9.42	2.38	6.55
E							E						
H	0.61						H	0.62					
C	0.2	1.07		Enrichment			C	0.19	1.07			Enrichment	
N	0.33	0.31	0.5				N	0.32	0.31	0.53			
O	3.46	0.68	0.06	0.1			O	3.47	0.68	0.06	0.11		
S	3.17	0.05	1.28	0	0		S	3.23	0.03	1.13	0	0	
HC	0.68	1.63	2.15	0.89	1.13	0.48	HC	0.68	1.64	2.15	0.89	1.16	0.48

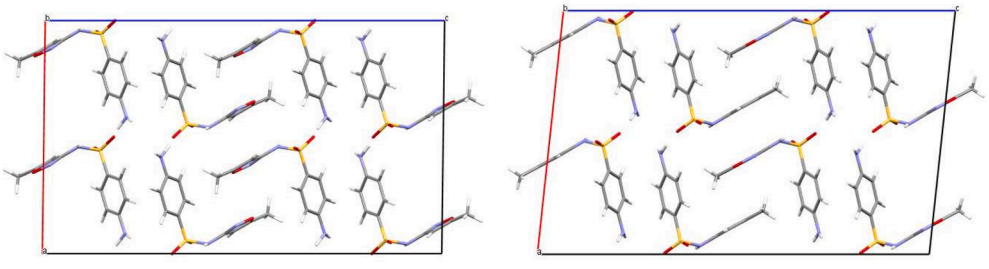

Fig. 6. Packing pattern in the unit cell of (a) Predicted and (b) Experimental crystal structures.

The third molecular pair contradicts the previous one, as 71 % of electrostatic and 29 % of dispersion energies contribute towards the total energy for the interaction N2-H4···O1 and C5-H5···O1. The average Etot values for the fourth and fifth molecular pairs were 31 KJ/mol [real] and 25 KJ/mol [DD], with 37 % and 63 % contributions of electrostatic and dispersion energies. On the whole, it was noted that molecular packing is highly stabilized by dispersion energies in both real and predicted crystal structures.

Table 6
Energy components (kJ/mol) for predicted DD structure (first line) and experimental (EXP) (second line) between the molecular pairs.

Symm.operator	Centroid Distance	E_{col}	E_{pol}	E_{dis}	E_{rep}	E_{tot}
x + 1/2, y + 1/2, z	8.33	−33.2	−6.1	−14.4	39.4	−27.9
	8.49	−14.2	−4.4	−9.6	10	−20.4
-x, y, -z + 1/2	13.25	2.4	−0.8	−3.7	1.1	−0.6
	12.75	0.7	−1.2	−6	3.8	−3
-x + 1/2, y + 1/2, -z + 1/2	8.74	−12	−2	−19.8	13.1	−23.3
	8.22	−16.7	−2.4	−24.3	15.8	−30.8
x, y, z	5.54	−16.6	−6.7	−28.9	25	−32.1
	5.48	−27.9	−9.1	−31.1	40.7	−38.2
-x, -y, -z	7.80	−10.8	−2.5	−28.7	18.5	−26.9
	7.17	−10.9	−3.6	−28.9	13.8	−30.9
-x + 1/2, -y + 1/2, -z	6.48	−13.1	−5	−41.2	24.5	−38.3
	6.65	−12.6	−3.5	−44	23.9	−39.4
-x, -y, -z	8.12	4.2	−0.7	−9	0.8	−3.4
	7.82	3.2	−1.2	−14.5	5.3	−7

Table 7
Topological properties of closed shell interactions of SMA in active site.

Bonds	ρ(r) eÅ^{-3}	$\nabla^2\rho(r)$ eÅ^{-5}	V(r) KJ/mol	G(r) KJ/mol	H(r) KJ/mol	E_{inter} KJ/mol
H1…THR62: OG1	0.19	1.93	−54.91	53.74	−1.16	−27.45
H7…ASP185: OD2	0.17	2.07	−50.28	53.32	3.04	−25.14
O1…ARG63: HH21	0.15	1.71	−44.51	45.52	1.01	−22.26
O2···.LYS221: HZ1	0.14	1.52	−41.45	41.41	−0.04	−20.72
O1···ARG255: HH12	0.10	1.14	−27.86	29.41	1.55	−13.93
N3…LYS221: HZ2	0.12	1.3	−28.8	30.3	1.6	−14.4
O1…ARG255: HH22	0.04	0.58	−10.20	12.97	2.78	−5.10
O1…ARG63: HE	0.03	0.49	−7.90	10.57	2.67	−3.95

Table 8
Topological properties obtained at B3LYP/*6–311++G*(d,*p*) of closed shell interactions of SMA in solid state.

Bonds	ρ(r) eÅ^{-3}	$\nabla^2\rho(r)$ eÅ^{-5}	V(r) KJ/mol	G(r) KJ/mol	H(r) KJ/mol	E_{inter} KJ/mol
C1-S1	1.39	−9.47	−526.61	134.34	−392.27	−263.31
C1-C2	2.04	−19.72	−1058.02	260.43	−797.59	−529.01
C2-C3	2.10	−20.71	−1113.11	274.49	−838.62	−556.55
C3-C4	2.04	−19.98	−1038.16	247.05	−791.11	−519.08
C4-C5	2.04	−19.98	−1037.49	246.64	−790.85	−518.74
C5-C6	2.09	−20.67	−1111.25	274.09	−837.17	−555.63
C6-C1	2.04	−19.70	−1057.67	260.53	−797.14	−528.83
C4-N2	2.07	−21.75	−1482.70	445.15	−1037.55	−741.35
S1-N1	1.44	−12.18	−877.95	273.07	−604.88	−438.97
N1-C7	2.00	−20.84	−1344.33	388.35	−955.97	−672.16
C7-N3	2.46	−24.70	−2177.25	752.25	−1425.00	−1088.63
N3-O3	2.08	−8.40	−1257.34	514.26	−743.08	−628.67
O3-C9	1.97	−5.25	−2067.15	962.11	−1105.04	−1033.57
C9-C8	2.21	−22.38	−1287.65	339.05	−948.60	−643.82
C8-C7	1.96	−18.08	−980.48	244.07	−736.42	−490.24
C9-C10	1.75	−15.50	−755.55	166.74	−588.81	−377.78
H4···O2	0.11	1.40	−29.22	33.61	4.39	−14.61
H7···O1	0.11	1.43	−29.81	34.38	4.58	−14.90
H1···O2	0.04	0.56	−9.43	12.36	2.93	−4.72

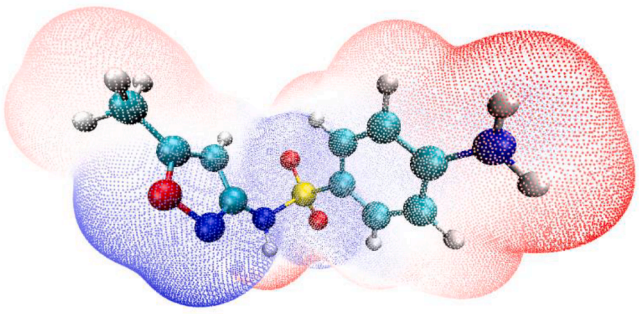

Fig. 7. Electrostatic potential maps plotted over the electron density isosurface at 0.001 au. Blue dots: Positive potential; Red dots: Negative potential. (For interpretation of the references to color in this figure legend, the reader is referred to the web version of this article.)

Table 9
Electrostatic energies of predicted and experimental crystal structures.

ID	E_{elect} [KJ/mol]
AK	−600.404
AH	−601.659
FC	−831.361
CA	−625.09
FA	−397.48
AM	−792.45
BF	−632.202
AV	−646.428
Exp	−1061.48
DD	−1061.9
AB	−677.808
CB	−487.854
CC	−481.997
AZ	−895.794
CE	−489.946
CD	−484.926
AP	−594.128
AY	−637.223
BH	−629.274
DB	−1356.03
AQ	−667.766
AS	−671.532
BB	−292.88
BA	−286.186
BD	−340.996
AA	−332.21
AF	−412.542
DA	−707.096
AU	−367.355

Closed shell interactions in the active and crystal phase

The strength of the intermolecular interactions between ligand and protein was validated from the electron density analysis using the QTAIM approach [12]. In the SMA-DHPS complex, the ρ(r) and $\nabla^2\rho(r)$ at bond critical point of all possible H-bond interactions were calculated using the Multiwfn package [26] and the values were listed in Table 7. The interaction energies were calculated based on Espinosa's relationship [27]. It is revealed that among the interactions, the NH group of the SMA ligand makes strong binding with the oxygen atom of THR62 residue with the energy value of −27.9 KJ/mol.

Moreover, a similar analysis was carried out for SMA molecule in the solid state from the search of (3,-1) type of critical point and the corresponding topological values calculated from B3LYP/6-311++G(d,p) level of theory were listed in Table 8. The impact of N—H···O interactions; N2-H4···O2, N2-H7···O1 and N1-H1···O2, in packing stability was well defined from their interaction energies and the values are −14.61 KJ/mol, −14.90 KJ/mol and −4.72 KJ/mol respectively.

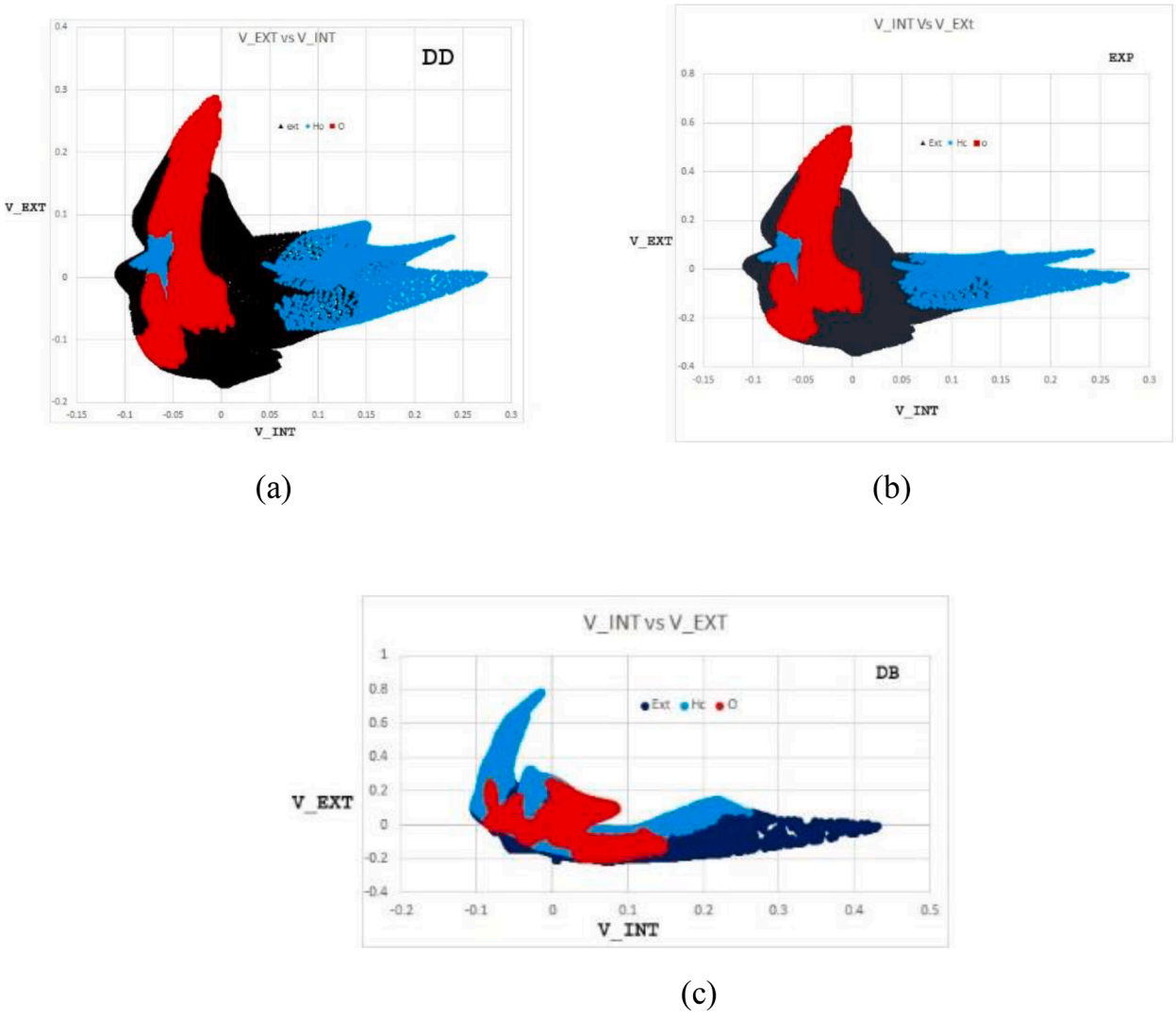

Fig. 8. Scatterplot of inner and outer electrostatic potential V on the Hirshfeld surface for crystal structures (a) DD, (b) EXP and (c) DB. The contacts donated by oxygen and by the hydrogen atom Hc from the inner molecule are highlighted in red and blue color, respectively. (For interpretation of the references to color in this figure legend, the reader is referred to the web version of this article.)

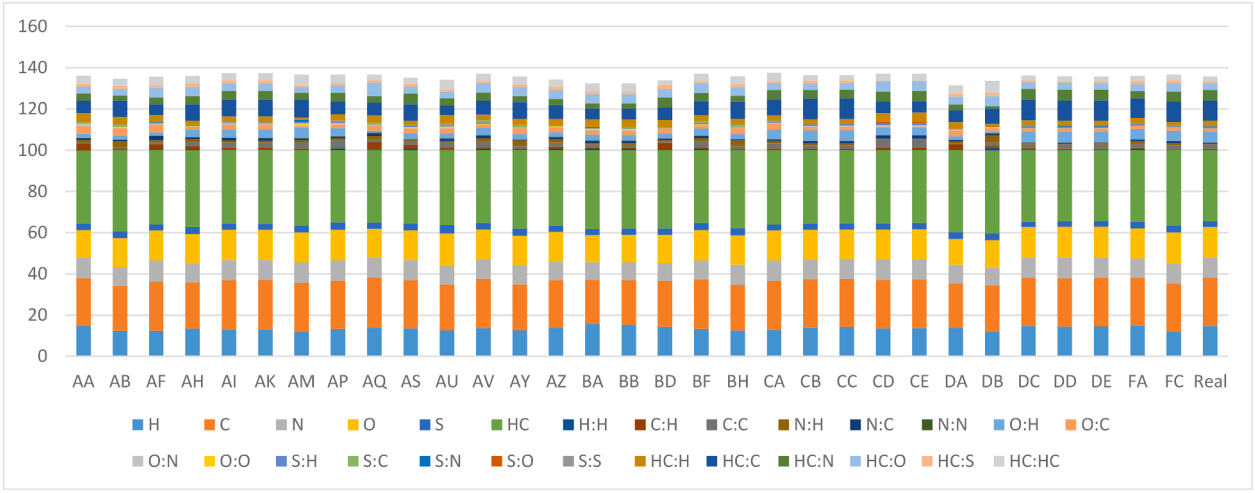

Fig. 9. Percentage of actual contacts in the real and predicted crystal packings.

Electrostatic potential of predicted structures

The polar characteristics of the SMA molecule lifted from the predicted crystal structure were established from molecular electrostatic potential (MESP) by evaluating the positive, V_{smax}, and negative extrema, V_{smin} potentials on the molecular surface using the program WFA-SAS [28]. The negative potential of the ligand in the active site was enhanced due to the interactions with the residues ARG63, LYS221, ARG255, THR62, and ASP185 [Fig. 7]. The donor and acceptor sites in the predicted structures were well identified from strong positive V_{smax} potential values for the atoms 443.57 KJ/mol and strong negative extrema, V_{smin} for the atoms 516.31 KJ/mol. Moreover, these values were in good agreement with those calculated for real crystal structures.

The electrostatic energy was calculated from the electron density multipolar model and the values are listed in Table 9 further it is computed that E_{elec} and Ul_{attice} values are correlated by 17 %.

Further, the correlation coefficient C_{VV} [Fig. 8] between interior and exterior potential was calculated for both experimental and predicted structures, which reveals the complementarity of inner and outer potential. In the experimental crystal structure, the polar hydrogen atoms lie in the regions of the highest inner potential and the oxygen atoms are at the origin of the electronegative areas. A similar trend was noted for predicted crystal structure. Among the predicted structures, DB has the highest E_{elec} energy and thus has an additional H-bond network when compared with experimental and DD crystal structures. In DB, the hydrogen atom of NH2 forms six H-bonds with the atoms O1, O3, N2, and N3. The C_{vv} correlation for the DB structure is −0.41 %, whereas the equivalent values for experimental and DD crystal structures were −0.12 %. The percentage of actual contacts in the real and predicted crystal packings is shown in Fig. 9.

Conclusion

The stable conformer of sulfamethoxazole was established from the various types of interactions with the amino acid residues ARG63, LYS221, ARG255, THR62, ASP185, PHE190, and PRO64 residues. The major contribution resulted from 10 hydrogen bonds framed by NH, NH_2, and SO_2 groups of a ligand with amino acid residues. The more stable packing was predicted and ranked the hypothetical structures based on the energy. From the energy landscape, it was determined that structure DD of spacegroup *C*2/*c* highly resembled with experimental structure with lattice energy of −145.91 KJ/mol. In both predicted and experimental crystal structure, the majority contact contribution towards the total HS surface is predicted from O···H/H···O interactions with 30.8 % and 32.8 % respectively. The closed shell interactions between the stable ligand and active site residues were characterized by QTAIM theory.

CRediT authorship contribution statement

David Stephen Arputharaj: Conceptualization, Methodology, Software. **Meenashi Rajasekaran:** Data curation, Writing – original draft. **P.V. Nidhin:** Visualization, Investigation.

Declaration of Competing Interest

The authors declare that they have no known competing financial interests or personal relationships that could have appeared to influence the work reported in this paper.

References

[1] L.H. Matherly, Molecular and cellular biology of the human reduced folate carrier, Prog. Nucleic Acid Res. Mol. Biol. 67 (2001) 131–162, https://doi.org/10.1016/s0079-6603(01)67027-2.
[2] O. Sköld, Sulfonamide resistance: mechanisms and trends, Drug Resist. Updat. 3 (2000) 155–160, https://doi.org/10.1054/drup.2000.0146.
[3] O. Sköld, Resistance to trimethoprim and sulfonamides, Vet. Res. 32 (2001) 261–273, https://doi.org/10.1051/vetres:2001123.
[4] D.I. Hammoudeh, Y. Zhao, S.W. White, R.E. Lee, Replacing sulfa drugs with novel DHPS inhibitors, Future Med. Chem. 5 (2013) 1331–1340, https://doi.org/10.4155/fmc.13.97.
[5] C. Capasso, C.T. Supuran, Sulfa and trimethoprim-like drugs - antimetabolites acting as carbonic anhydrase, dihydropteroate synthase and dihydrofolate reductase inhibitors, J. Enzyme Inhib. Med. Chem. 29 (2014) 379–387, https://doi.org/10.3109/14756366.2013.787422.
[6] B.L. Strom, R. Schinnar, A.J. Apter, D.J. Margolis, E. Lautenbach, S. Hennessy, W. B. Bilker, D. Pettitt, Absence of cross-reactivity between sulfonamide antibiotics and sulfonamide nonantibiotics, N. Engl. J. Med. 349 (2003) 1628–1635, https://doi.org/10.1056/NEJMoa022963.
[7] D. Fernández-Villa, M.R. Aguilar, L. Rojo, Folic acid antagonists: Antimicrobial and immunomodulating mechanisms and applications, Int. J. Mol. Sci. 20 (2019) 1–30, https://doi.org/10.3390/ijms20204996.
[8] C.F. Stratton, H.A. Namanja-Magliano, S.A. Cameron, V.L. Schramm, Binding isotope effects for para-aminobenzoic acid with dihydropteroate synthase from Staphylococcus aureus and Plasmodium falciparum, ACS Chem. Biol. 10 (2015) 2182–2186, https://doi.org/10.1021/acschembio.5b00490.
[9] X. Wen, J. Sheng Wang, J.T. Backman, J. Laitila, P.J. Neuvonen, Trimethoprim and sulfamethoxazole are selective inhibitors of CYP2C8 and CYP2C9, respectively, Drug Metab. Dispos. 30 (2002) 631–635, https://doi.org/10.1124/DMD.30.6.631.
[10] M.-K. Yun, Y. Wu, Z. Li, Y. Zhao, M.B. Waddell, A.M. Ferreira, R.E. Lee, D. Bashford, S.W. White, Catalysis and sulfa drug resistance in dihydropteroate synthase, Science 335 (2012) 1110–1114, https://doi.org/10.1126/science.1214641.
[11] W.T. Hughes, J. Killmar, Monodrug efficacies of sulfonamides in prophylaxis for Pneumocystis carinii pneumonia, Antimicrob. Agents Chemother. 40 (1996) 962–965, https://doi.org/10.1128/aac.40.4.962.
[12] R.F.W. Bader, Atoms in Molecules: A Quantum Theory, Oxford University Press, 1990, p. 438, accessed October 27, 2022.
[13] G. Madhavi Sastry, M. Adzhigirey, T. Day, R. Annabhimoju, W. Sherman, Protein and ligand preparation: parameters, protocols, and influence on virtual screening enrichments, J. Comput. Aided. Mol. Des. 27 (2013) 221–234, https://doi.org/10.1007/S10822-013-9644-8.
[14] Schrödinger, LigPrep, (2020) 1.
[15] M. Xu, M.A. Lill, Induced fit docking, and the use of QM/MM methods in docking, Drug Discov. Today Technol. 10 (2013) e411–e418, https://doi.org/10.1016/J.DDTEC.2013.02.003.
[16] The PyMOL Molecular Graphics System, Version 1.2r3pre, Schrödinger, LLC, (n.d.).
[17] P. Geerlings, F. De Proft, W. Langenaeker, Conceptual density functional theory, Chem. Rev. 103 (2003) 1793–1873, https://doi.org/10.1021/CR990029P/ASSET/CR990029P.FP.PNG_V03.
[18] 2016. Gaussian 09, Revision A.02, M. J. Frisch, G. W. Trucks, H. B. Schlegel, G. E. Scuseria, M. A. Robb, J. R. Cheeseman, G. Scalmani, V. Barone, G. A. Petersson, H. Nakatsuji, X. Li, M. Caricato, A. Marenich, J. Bloino, B. G. Janesko, R. Gomperts, B. Mennucci, No Title, (n.d.).
[19] J.R. Holden, Z. Du, H.L. Ammon, Prediction of possible crystal structures for C-, H-, N-, O-, and F-containing organic compounds, J. Comput. Chem. 14 (1993) 422–437, https://doi.org/10.1002/JCC.540140406.
[20] S.L. Price, M. Leslie, G.W.A. Welch, M. Habgood, L.S. Price, P.G. Karamertzanis, G. M. Day, Modelling organic crystal structures using distributed multipole and polarizability-based model intermolecular potentials, Phys. Chem. Chem. Phys. 12 (2010) 8478–8490, https://doi.org/10.1039/C004164E/.
[21] D.E. Williams, S.R. Cox, Nonbonded potentials for azahydrocarbons: the importance of the Coulombic interaction, Urn:Issn:0108–7681. 40 (1984) 404–417, https://doi.org/10.1107/S010876818400238X.
[22] D.S. Coombes, S.L. Price, D.J. Willock, M. Leslie, Role of electrostatic interactions in determining the crystal structures of polar organic molecules. A distributed multipole study, J. Phys. Chem. 100 (1996) 7352–7360, https://doi.org/10.1021/jp960333b.
[23] A. Stone., The Theory of Intermolecular Forces, International Series of Monographs on Chemistry Oxford University Press, Oxford, 1996.
[24] G.L. Perlovich, A.M. Ryzhakov, V.V. Tkachev, L.K. Hansen, O.A. Raevsky, Sulfonamide molecular crystals: Structure, sublimation thermodynamic characteristics, molecular packing, hydrogen bonds networks, Cryst. Growth Des. 13 (2013) 4002–4016, https://doi.org/10.1021/cg400666v.
[25] P.R. Spackman, M.J. Turner, J.J. McKinnon, S.K. Wolff, D.J. Grimwood, D. Jayatilaka, M.A. Spackman, CrystalExplorer: a program for Hirshfeld surface analysis, visualization and quantitative analysis of molecular crystals, Urn:Issn: 1600–5767. 54 (2021) 1006–1011, https://doi.org/10.1107/S1600576721002910.
[26] T. Lu, F. Chen, Multiwfn: A multifunctional wavefunction analyzer, J. Comput. Chem. 33 (2012) 580–592, https://doi.org/10.1002/jcc.22885.
[27] E. Espinosa, E. Molins, C. Lecomte, Hydrogen bond strengths revealed by topological analyses of experimentally observed electron densities, Chem. Phys. Lett. 285 (1998) 170–173, https://doi.org/10.1016/s0009-2614(98)00036-0.
[28] F.A. Bulat, A. Toro-Labbé, T. Brinck, J.S. Murray, P. Politzer, Quantitative analysis of molecular surfaces: areas, volumes, electrostatic potentials and average local ionization energies, J. Mol. Model. 16 (2010) 1679–1691, https://doi.org/10.1007/S00894-010-0692-X.